Fabrication and electrochemical properties of porous carbon/$LiFePO_4$ composite nanostructure

Nipaporn Bamrungna[a], Areerat Nilrut[a], Pailyn Thongsanitgarn[a], Wanwisa Limphirat[b], Sukanya Nilmoung[a,*]

[a] Department of Applied Physics, Faculty of Sciences and Liberal Arts, Rajamangala University of Technology Isan, Nakhon Ratchasima, 30000 Thailand
[b] Synchrotron Light Research Institute (Public Organization), Nakhon Ratchasima, 30000 Thailand

***Corresponding Author:** sukanya.ni@rmuti.ac.th
https://doi.org/10.55674/jmsae.v11i3.251712

Received: 4 February 2023 | **Revised:** 13 February 2023 | **Accepted:** 27 September 2024 | **Available online:** 1 September 2024

Abstract

This work reports the synthesis and electrochemical properties of porous carbon composite with lithium iron phosphate ($LiFePO_4$) for use as electrode materials in energy storage devices. Two forms of carbon were prepared; including activated carbon (AC) and carbon nanofibers (ACNF). The ACNF/$LiFePO_4$ composite nanostructure was fabricated by electrospinning while the AC/$LiFePO_4$ composite nanostructure was obtained by the sol-gel method followed by the heat treatment process. All samples were characterized by X-ray diffraction (XRD), scanning electron microscopy (SEM), transmission electron microscopy (TEM), and Brunauer-Emmett-Teller analyzer (BET). The electrochemical properties were tested using cyclic voltammetry (CV) and galvanostatic charge-discharge at various current densities (0.25 – 10 Ag^{-1}) and various C-rates (0.20 – 5 C). The AC/$LiFePO_4$ electrode showed better electrochemical properties than those of the ACNF/$LiFePO_4$ electrode. A maximum specific capacitance of 82 F g^{-1} at 2 m Vs^{-1} and initial discharge capacities of 45 mA hg^{-1} at 0.20 C were observed. Moreover, the AC/$LiFePO_4$ electrode showed better cycle performance than that of the ACNF/$LiFePO_4$ electrode at all C-rates. The interesting electrochemical properties of AC/$LiFePO_4$ composite nanostructure make it a potential candidate for use as electrode materials in energy storage devices.

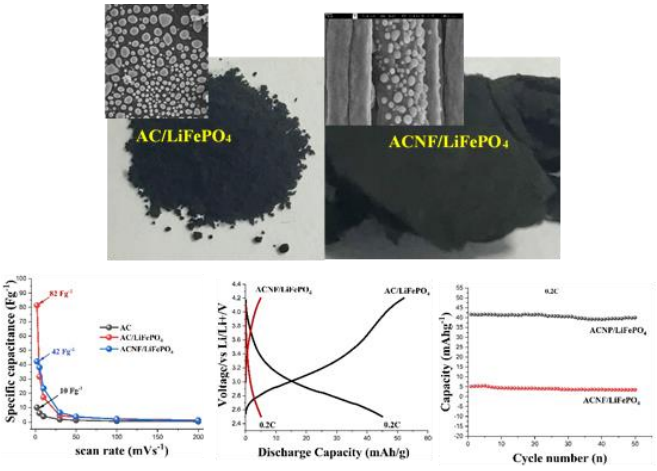

Keywords: Porous carbon; $LiFePO_4$; Electrochemical properties; Electrospinning; Energy storage devices

Introduction

With the world's growing population and the global energy crisis, especially electrical energy, the demand for alternative energy resources has been of interest. Currently, the demand for electrical energy storage systems is growing in parallel with the need for electrical vehicles (EVs). Among energy storage devices, lithium-ion batteries (LIB) are the dominant sustainable energy storage devices due to their high energy density and low self-discharge rate [1]. It is well known that high-efficiency electrode material plays an important role in determining the characteristics of these devices. Therefore, improved energy density and cycling stability of electrode materials has become a breakthrough challenge for researchers. Various cathode materials such as $LiCoO_2$, $LiMn_2O_4$, $LiNiO_2$, etc. have been previously reported [2, 3]. $LiFePO_4$ is an olivine structure and was first reported as a cathode material for lithium-ion batteries in 1997 [4]. This material has attracted much attention because of its high theoretical capacity170 mA·hg^{-1} [5], high thermal stability and low toxicity [6]. Unfortunately, low electronic conductivity (10^{-9} – 10^{-10} cm^2 S^{-1}) and poor lithium-ion diffusion coefficient (1.80 × 10^{-18} m^2 s^{-1}) lead to poor electrochemical properties [7 – 9]. From this perspective, the

development of high conductivity and high ion diffusion rate of $LiFePO_4$ has been imperative. Currently, several methods are being used, for example: reducing particle size to reduce the path length of lithium-ion diffusion [10], doping with metal ions as multi-functional hybrid materials to increase the electronic conductivity [11, 12], and coating with conductive carbonaceous materials [13]. Carbon is the most desirable material due to its coating tunable surface chemistry [14]. Various forms of carbon have been fabricated for use as electrode materials in energy storage devices, including carbon nanotubes, carbon nanofibers, graphene, graphite, carbon aerogel, etc [15 − 18]. Activated carbon is a form of carbon that has been processed to have small and low-volume pores. Such behavior enhances the surface area for the imbedding of ions which significantly boosts the specific capacitance. Moreover, the high conductivity of activated carbon is necessary to prevent energy loss during the charge/discharge process. Both unique properties of activated carbon are suited to serve as an electrode material for energy storage devices than other carbon forms.

Herein, porous carbon in the form of activated carbon (AC) and activated carbon nanofiber (ACNF) composite with lithium iron phosphate (AC/$LiFePO_4$, ACNF/$LiFePO_4$ composite nanostructure) were fabricated for use as cathode material in LIB. The influence of carbon forms on the composite nanostructure's structure, morphology, and electrochemical performance of the composite nanostructure was discussed in detail.

Materials and Methods

Chemicals

Iron (III) nitrate nonahydrate ($Fe(NO_3)_3(H_2O)_9$, Sigma-Aldrich), lithium phosphate monobasic (LiH_2PO_4, Sigma-Aldrich), Polyacrylonitrile ($(C_3H_3N)_n$ Sigma-Aldrich), N, N-dimethylformamide anhydrous ($HCON(CH_3)_2$, SIAL), and polyethylene glycol ($H(OCH_2CH_2)$Noh, Sigma-Aldrich) were used as the precursor substances for preparing the composite materials. Carbon black (C, Alfa Aesar) polyvinylidene difluoride ($(CH_2CF_2)_n$, Sigma-Aldrich), and 1-Methyl-2pyrolidinone (C_5H_9NO, Sigma-Aldrich) were used as the substance for working electrode preparation. Potassium hydroxide (KOH, Sigma-Aldrich) was used as the electrolyte in a three-electrode testing system. Lithium hexafluorophosphate solution was used as an electrolyte in coin cells.

Synthesis of ACNF/ $LiFePO_4$ composite nanostructures

The ACNF/$LiFePO_4$ composite nanostructures were prepared by electrospinning technique followed by stabilization, carbonization, and activation processes, respectively. For the synthesis, a 2.10 g of polyacrylonitrile was dispersed into 25 ml of DMF solvent for use as the carbon source, whereas the $LiFePO_4$ source was prepared by mixed lithium phosphate monobasic and Iron (III) nitrate nonahydrate in 2:1 M in 5 mL of DMF. Both sources were mixed and converted into fibers via an electrospinning technique. An applied voltage of 14 kV and a feeding rate of 0.30 mlh^{-1} was operated in the electrospinning system. The fibers were dried at 60°C for 48 h and then, transfer to the heat treatment process as follows: stabilized at 300°C for 4 h in the air atmosphere, carbonized at 700°C for 2 h in the argon atmosphere, and activated at 800°C for 30 min in the carbon dioxide atmosphere. Finally, the ACNF/$LiFePO_4$ composite nanostructure was obtained.

Synthesis of AC/ $LiFePO_4$ composite nanostructures

The AC/$LiFePO_4$ powder was synthesized by the sol-gel method followed by carbonization, and activation processes, respectively. Both sources of precursor solution were prepared in a similar way to the ACNF/$LiFePO_4$ composite nanostructures. After mixed of both source solutions, 2 g of polyethylene was added to generate a gel solution. The prepared gel was carbonization at 700°C for 12 h in an argon atmosphere followed by activated at 800°C for 1 h in a carbon dioxide atmosphere. The final product was designated as AC/$LiFePO_4$.

Materials characterization

The crystalline phases of prepared samples were evaluated using X-ray powder diffraction (XRD, Bruker D2 advance). The surface area was observed using the Brunauer-Emmett-Teller analyzer (BET, BEL SORP MINI II, JAPAN). The particle size and morphology were investigated using field emission scanning electron microscopy (FE-SEM, Carl Zeiss, Auriga) and was confirmed using transmission electron microscopy (TEM, FEI Tecnai G^2, USA). The Selected area electron diffraction (SAED) patterns were also detected.

Electrochemical characterization

The electrochemical performance of the working electrode was tested using cyclic voltammetry (CV) and galvanostatic charge-discharge (GCD) via autolab (PG

STAT 302N, Metrohm). Three-electrode system under a 6 M KOH electrolyte solution was used**.** An active sample powder, carbon black, and polyvinylidene difluoride with a weight ratio of 8:1:1 was used for preparing the working electrode. Mixed powder in NMP solvent was coated onto Ni foam substrate, dried at 90°C overnight, and then pressed to get a working electrode. The cyclic voltammetry was scanned in the potential window of -1.10 – 1.20 V at rates of 2 – 200 m Vs^{-1}. The galvanostatic charge/discharge with a current density of 0.25 – 10 Ag^{-1} was used to measure between the selected potential windows. Moreover, coin cell batteries (CR2032) were prepared for galvanostatic charge-discharge measurement. A mixture of the prepared sample (ACNF/$LiFePO_4$ or AC/$LiFePO_4$), poly (vinyl difluoride) (PVDF), and acetylene black (at the ratio of 8:1:1, wt%) was coated onto Al foil and then dried at 90°C overnight. Celgard 2400 membrane and lithium foil were used as the separator and negative electrode, respectively. The electrolyte 1 M LiPF6 was dispersed in a 1:1 (v/v) mixture of ethylene carbonate (EC)/dimethyl carbonate (DMC). The galvanostatic charge-discharge cycling of coin cells was conducted at the voltage between 2.50 and 4.20 V at C-rates of 0.20-5C via a battery testing station (Neware, BTS4000).

Results and Discussions

Fig**.** 1 shows the XRD pattern of AC/$LiFePO_4$ and ACNF/$LiFePO_4$ composite nanostructures carbonized at 700°C**.** The characteristic peaks at 2θ of ACNF/$LiFePO_4$ composite nanostructures were attributed to the reflections of (200), (101), (210), (111), (211), (301), (311), (121) (410) (002) (112) (321) (212) (022) (131) (222) (412) (331) and (620), respectively, crystalline plan of orthorhombic $LiFePO_4$ (PDF card no. 01-081-1173) [19]**.** A few asterisks in thexrd pattern (*) showed some accompanying impurities are often unavoidable for $LiFePO_4$. For AC/$LiFePO_4$ composite nanostructures, some diffraction peaks ((212) (131) and (331)) could not be detected, which may be ascribed to either the high content of the carbon phase or low content $LiFePO_4$ phase. The crystallinity percentage of $LiFePO_4$ was calculated by dividing the area of crystalline peaks by the area of all peaks and multiplying the result by 100. The values of 63.20% and 53.70% were observed for AC/$LiFePO_4$ and ACNF/$LiFePO_4$, respectively. Moreover, the crystallite size (D) of $LiFePO_4$ was calculated by the Scherrer equation. The values of 41 and 47 nm were observed for AC/$LiFePO_4$ and ACNF/$LiFePO_4$, respectively. The diffraction plan (002) at about 25° can be ascribed to the graphitized structure in JCPDS card no**.** 75-1621 [20]**.** The broad peak characteristic indicated amorphous carbon [21].

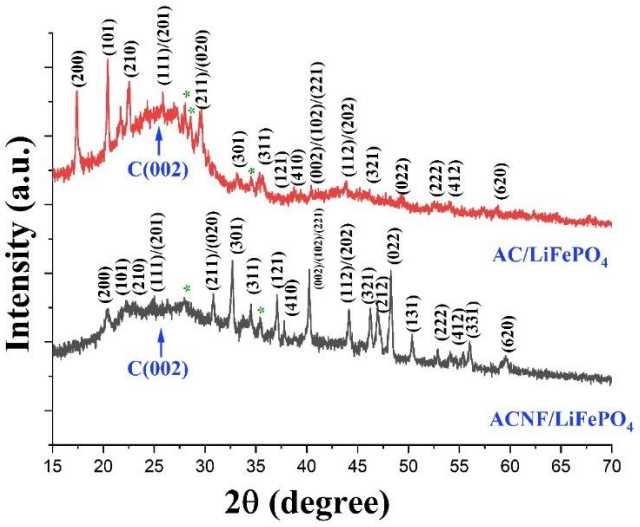

Fig. 1 XRD patterns of the ACNF/$LiFePO_4$ and AC/$LiFePO_4$ composite nanostructures.

Fig. 2 shows the morphologies of ACNF/$LiFePO_4$ and AC/$LiFePO_4$ composite nanostructures carbonized at 700°C. The ACNF/$LiFePO_4$ composite nanostructure revealed long straight fiber, smooth and uniform in cross-section with an average diameter of ~260 nm. Uniform $LiFePO_4$ particles with a spherical shape and an average size of 77 nm were embedded in carbon fibers (Fig. 2 (a), (c), (e))**.** Non-woven carbon nanofibers may possibly not form a continuous network thus limiting the growth of $LiFePO_4$ nanoparticles. However, small-sized $LiFePO_4$ can be beneficial in shortening the diffusion path of ions and enhancing the effective reaction areas between particles and electrolytes [22]. The AC/$LiFePO_4$ composite nanostructure exhibited a carbon matrix embedded with uniform spherical $LiFePO_4$ particles with an average size of 154 nm (Fig. 2 (b)). It is well known that different methods of synthesis cause different sizes of $LiFePO_4$ particles. For example, 50 – 100 nm by solid-state route [23], 100 – 200 nm by hydrothermal [24], and colloidal process [25]. It was expected that our prepared samples in nanoscale would offer a short length for charge diffusion and thus improve the high specific capacitance and cycling stability of the electrode.

Fig. 3 shows TEM images and SAED patterns of both prepared samples. The TEM images of the ACNF/$LiFePO_4$ composite nanostructure showed clearly that the $LiFePO_4$ nanoparticles with spherical shape were embedded within the activated carbon nanofiber (ACNF) (Fig. 3 (a)). The

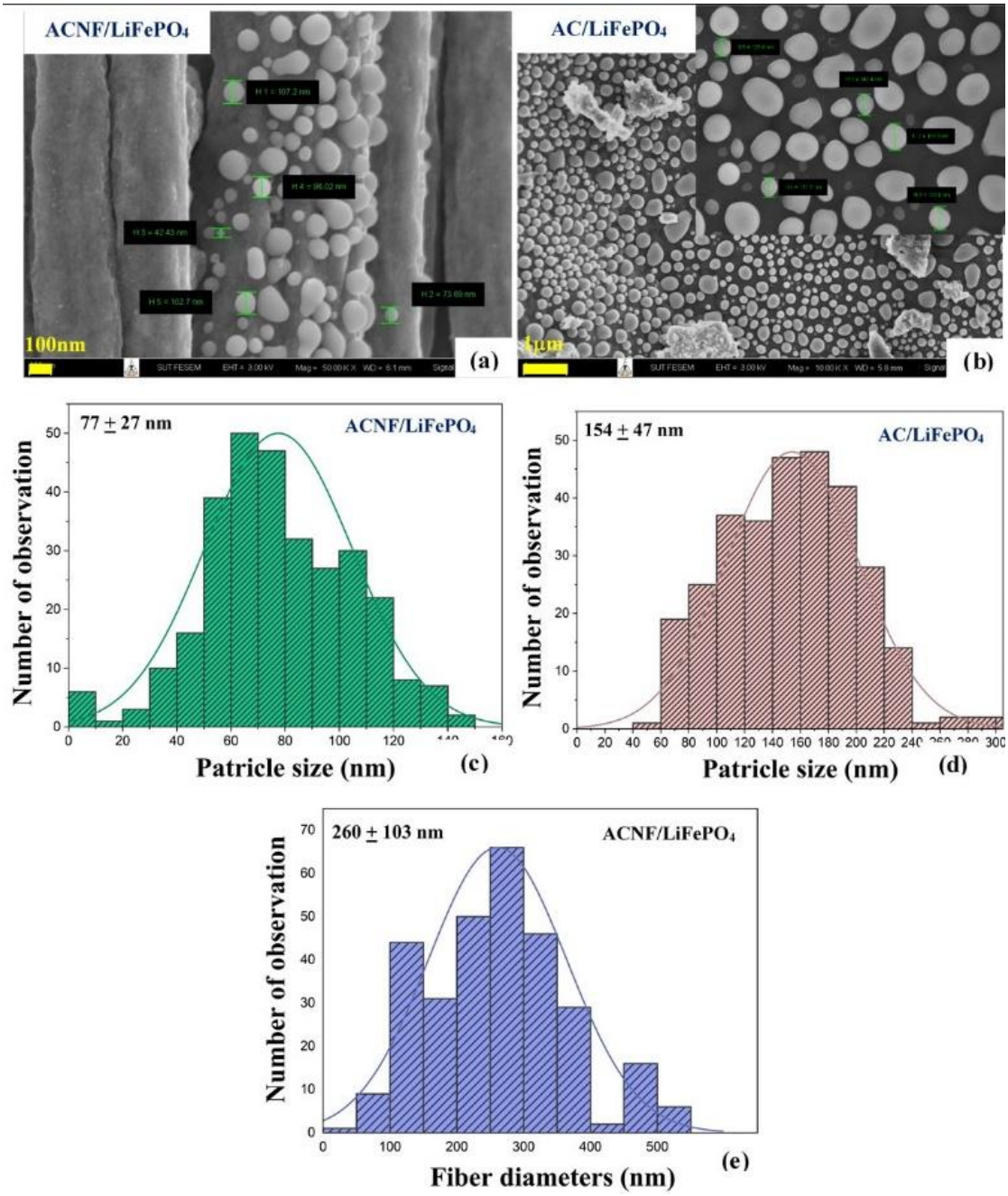

Fig. 2 (a) SEM images and the histograms of (c) particle size and (e) fiber diameter for the ACNF/$LiFePO_4$ composite nanostructure. (b) SEM images and (d) the histograms of particle size for the AC/$LiFePO_4$ composite nanostructures.

average particle size of $LiFePO_4$ measured from the TEM image was 80 nm. The corresponding SAED patterns showed diffraction spots which could be indexed to the high crystallinity of $LiFePO_4$ (Fig. 3 (c)). For AC/$LiFePO_4$ composite nanostructure, the carbon matrix was embedded with $LiFePO_4$ nanoparticles with an average size of 110 nm (Fig. 3 (b)). No spotty rings were observed in the SAED patterns of the activated carbon area, which suggested the large amorphous characteristics of carbon (Fig. 3 (d)).

Fig. 4 shows the N_2 adsorption/desorption isotherm of the AC/LiPFePO_4 (Fig. 4 (a)) and ACNF/LiPFePO_4 (Fig. 4 (b)) composite nanostructures. The sample showed a typical type-IV isotherm with a small degree of the hysteresis loop,

indicating the presence of a mesoporous structure [26]. The pore size distribution is shown as an inset. The AC/$LiFePO_4$ showed a predominant peak at 19 nm, whereas ACNF/$LiFePO_4$ displayed a peak at approximately 27 nm.

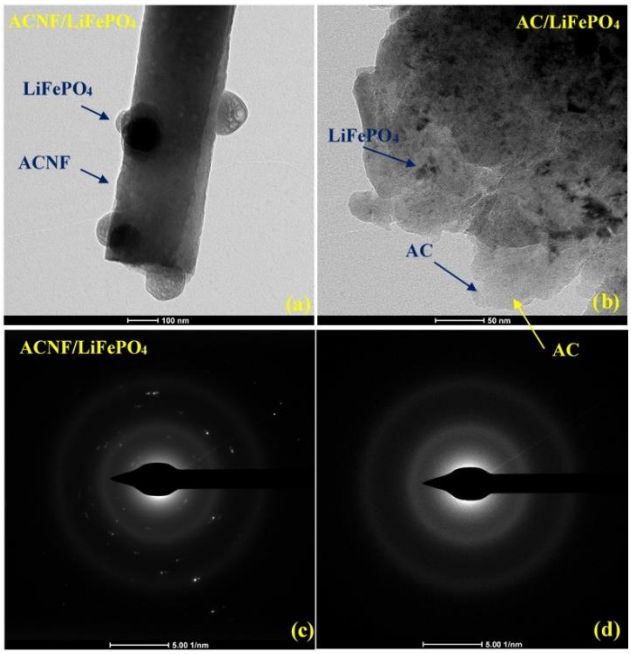

Fig. 3 TEM images of the ACNF/$LiFePO_4$ (a) and the AC/$LiFePO_4$ (b) composite nanostructure. The SAED patterns of ACNF/$LiFePO_4$ (c) and the AC area of AC/$LiFePO_4$ composite nanostructure (d).

The specific surface areas of 41.78 and 106.43 $m^2\,g^{-1}$ were observed for ACNF/$LiFePO_4$ and AC/$LiFePO_4$, respectively. In this study, a large value of the surface area was required in order to possess more active sites, provide high accessibility to electrolyte ions and facilitate fast ions transfer between electrode and electrolyte. The summary of specific surface area, average pore size, and total pore volume are presented in Table. 1.

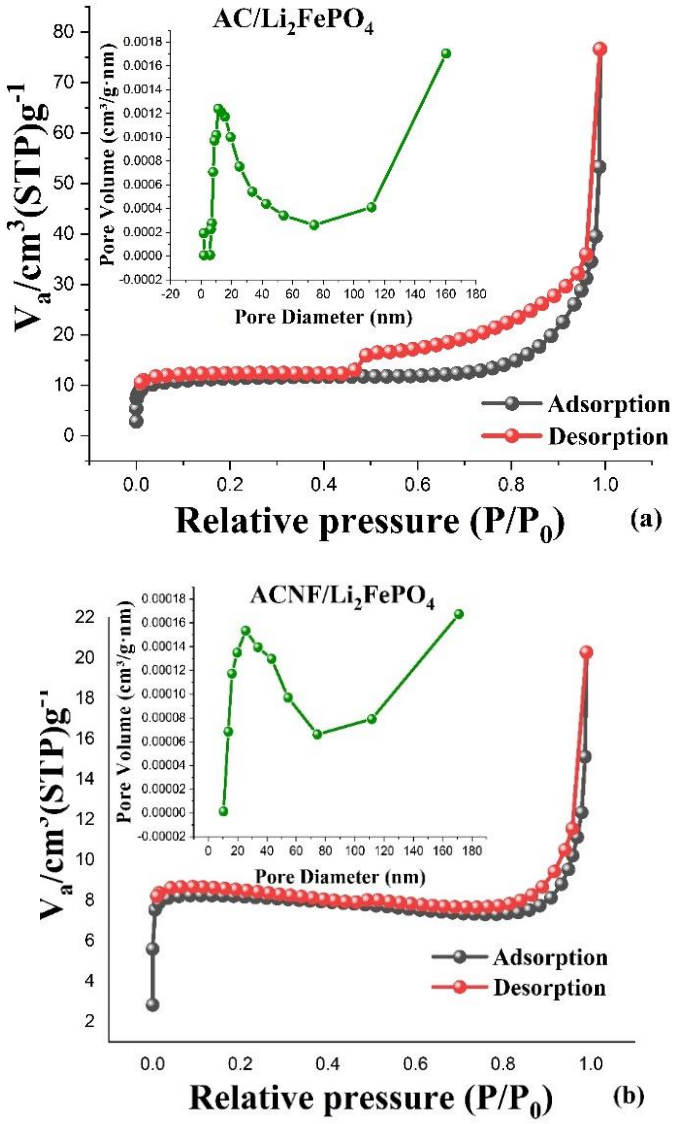

Fig. 4 N_2 adsorption-desorption isotherm and BJH pore size distribution plot (inset) of (a) AC/LiPFePO_4 and (b) ACNF/LiPFePO_4 composite nanostructures.

Table. 1 lists of surface area (a), average pore size (r_{ave}), pore volume (V_p), average fiber diameter (f_{ave}), $LiFePO_4$ size (d_{ave}), specific capacitance (C_s), and the first discharge capacities (C_{1s}) of prepared samples.

samples	A (m^2g^{-1})	r_{ave} (nm)		V_p (cm^3g^{-1})	f_{ave} (nm)	d_{ave} (nm)	C_s (Fg^{-1}) 2mVs^{-1}	C_{1s} ($mAhg^{-1}$) 0.20C
		adsorption	desorption					
ACNF/$LiFePO_4$	41.78	65.82	35.89	0.02	260	77	42	5.20
AC/$LiFePO_4$	106.43	44.19	17.28	0.10	-	154	82	45

Fig. 5 shows CV curves over a voltage range of –1 to –1.20 V for activated carbon, AC/$LiFePO_4$, and ACNF/$LiFePO_4$ composite nanostructures. The CV curves for pristine activated carbon (AC) were also measured for comparison. The rounding of CV curve corners with small redox peaks inferred the charge storage behavior of the carbonaceous material with resistances (EDLC) and metal oxides (pseudocapacitance) [16]. The magnitude of pseudocapacitance is markedly larger than EDLC. This is because charge storage in pseudocapacitors occurs by means of redox reaction throughout the bulk of the electrode material while it occurs only at the surface in EDLC [27]. The CV curves increased with an increase in the scan range suggesting the high rate capability of materials. The specific capacitance from the CV curve was calculated by equation (1)

$$C_s = \int \frac{IdV}{m\nu\Delta V} \quad (1)$$

where $\int$ IdV is the area under the CV curve, ν is the scan rate, m is the prepared active mass, and ΔV is the potential window. The calculation results show that the specific capacitance decreased with an increase in the scan rate (Fig. 5 (d). A lower capacitance at higher scan rates is due to none sufficient time for electrolyte ions to penetrate into the electrode materials [28]. Interestingly, the AC/$LiFePO_4$ showed higher values than those of the ACNF/$LiFePO_4$ and pristine AC at low scan rates (2 – 50 m

Fig. 6 displays GCD spectra for AC/$LiFePO_4$ (Fig. 6 (a)) and ACNF/$LiFePO_4$ (Fig. 6 (b)) electrodes. The GCD spectra deviating from a straight line mainly came from the redox

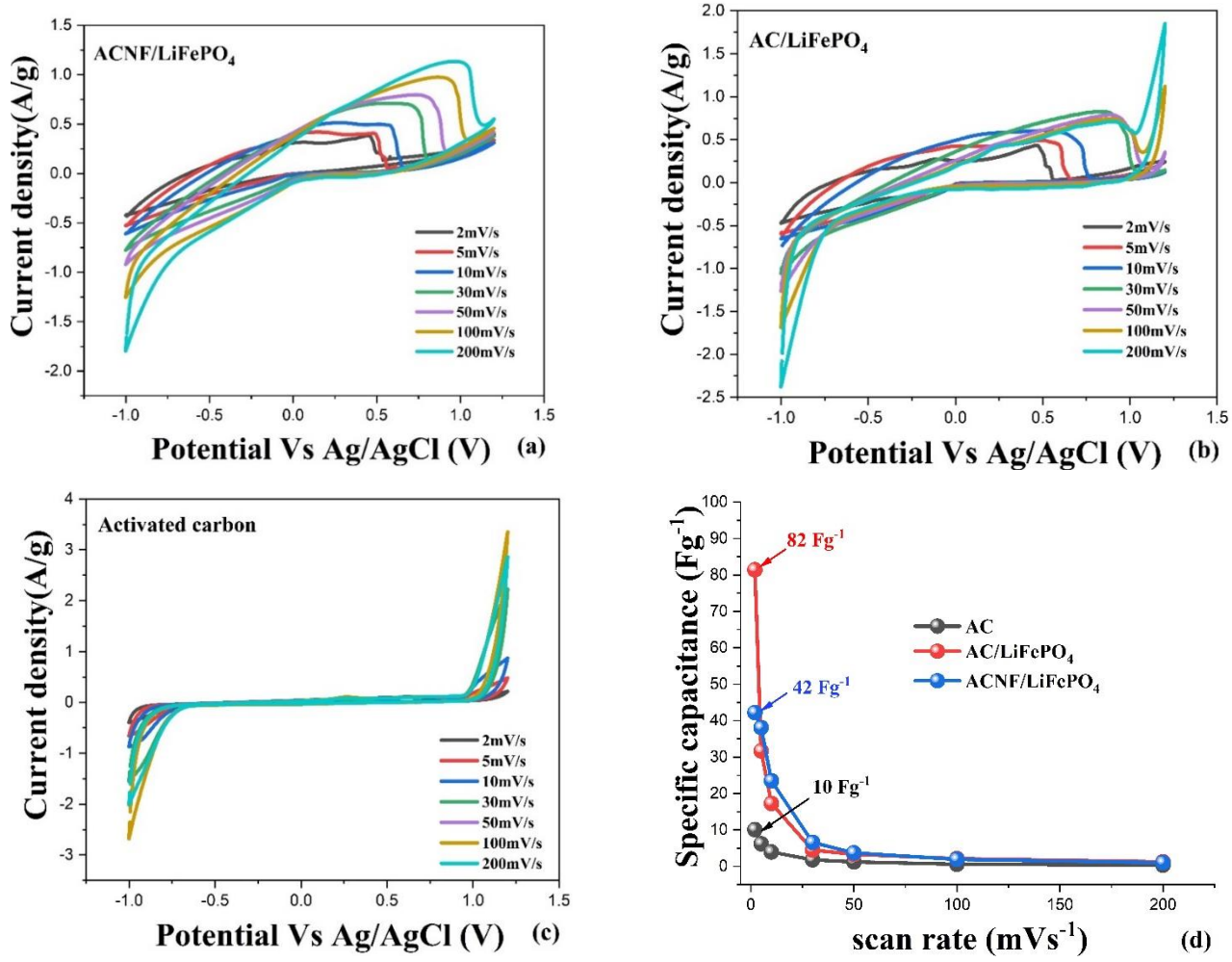

Fig. 5 (a) Cyclic voltammetry curves for the ACNF/$LiFePO_4$, (b) AC/$LiFePO_4$, (c) Pristine activated carbon and (d) The corresponding specific capacitance.

reactions of metal oxide [29]. No IR drop was observed indicating good electrochemical stability and implying that the composite material had a good capacitive characteristic [14]. From the GCD spectra, the specific capacitance can be calculated based on equation (2)

$$C_s = \frac{It}{mV} \quad (2)$$

where I is the constant current, t is the discharge time, m is the active mass of electrode material, and V is the potential window. The charge/discharge time of AC/LiFePO$_4$ spectra was longer than that of ACNF/LiFePO$_4$ as clearly seen at a current density of 0.25 Ag^{-1} (Fig. 6 (c)). Such a result indicated higher specific capacitance of AC/LiFePO$_4$ compared to ACNF/LiFePO$_4$ electrode and well agreed with CV results. Fig. 7 (a) and (c) show the first charge/discharge profiles between 2.50 – 4.20 V at various C-rates (0.20 – 5 C) for AC/LiFePO$_4$ and ACNF/LiFePO$_4$ electrodes, respectively. Almost no plateau region was observed in the ACNF/LiFePO$_4$ electrode spectra, while a short plateau with a large slope region as the capacitive behavior at the reaction interface was observed for AC/LiFePO$_4$. Such behavior has been reported for nanomaterials with high surface area [30 – 31]. The initial discharge capacities of 45, 39, 29, 19, and 5 mA hg^{-1} for AC/LiFePO$_4$ electrodes were observed at 0.20, 0.50, 1, 2, and 5 C, respectively. Meanwhile, the initial discharge capacities of the ACNF/LiFePO$_4$ electrodes were 5.20, 2.90, 1.47, 0.78, and 0.30, mA hg^{-1}, respectively.

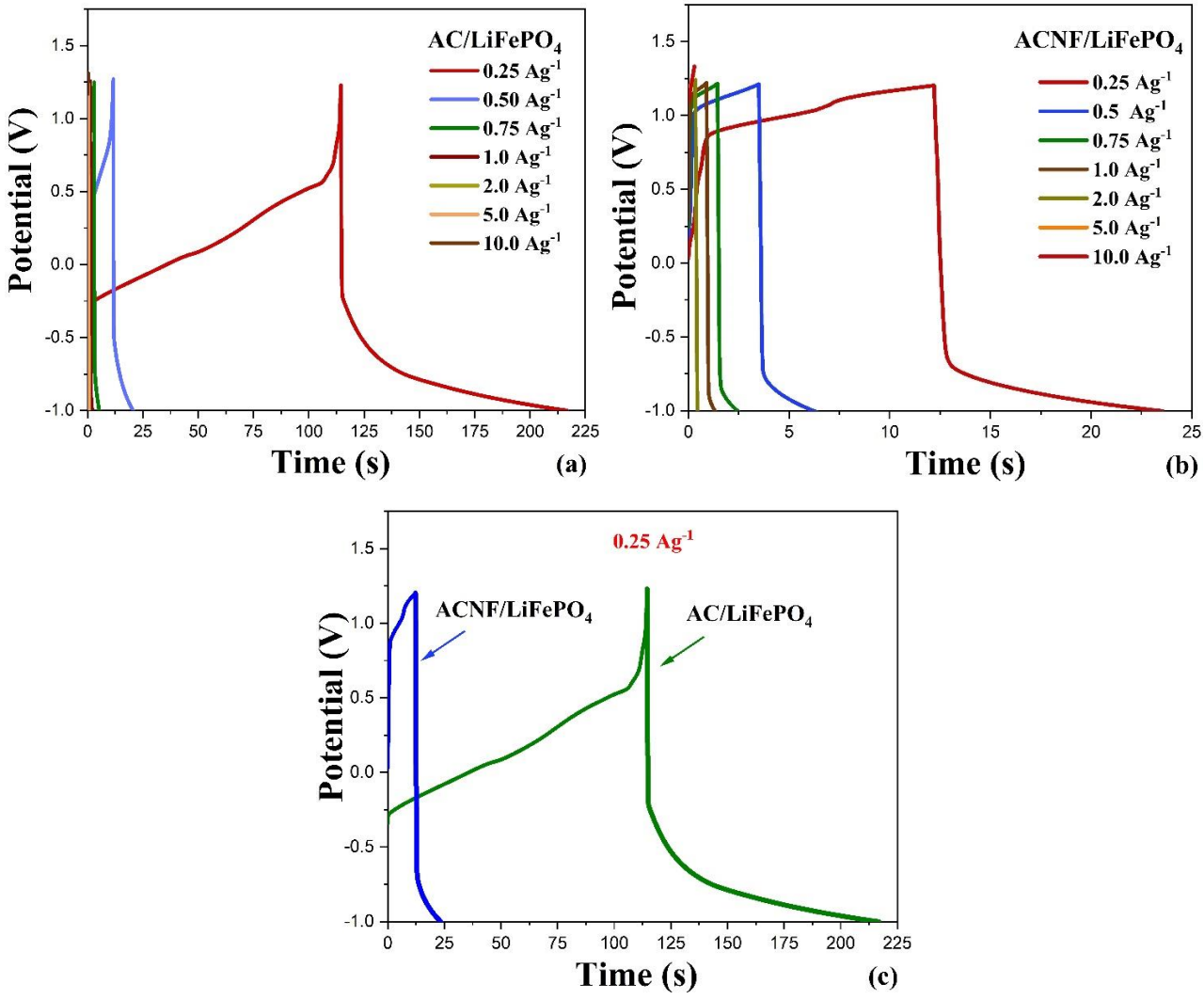

Fig. 6 GCD spectra at various current densities (0.25 – 10.0 Ag^{-1}) for (a) AC/LiFePO$_4$ and (b) ACNF/LiFePO4 electrodes. (c) GCD spectra at a current density of 0.25 Ag^{-1}.

The low electrochemical performance of ACNF/$LiFePO_4$ might have been from non-woven carbon nanofibers providing slow electronic transport during charge-discharge processes. The rate performance at 0.20 – 5 C of AC/$LiFePO_4$ and ACNF/$LiFePO_4$ composite materials are shown in Fig.7 (b) and (d), respectively. It was found that the AC/$LiFePO_4$ electrode showed better discharge capacity than that of the ACNF/$LiFePO_4$ electrode at all C-rates. Such behavior may have been due to the activation carbon (AC) providing more sites for $LiFePO_4$ and constructing continuous pathways for electrons compared to activated carbon nanofiber (ACNF). These facilitated the movement of electrons from all directions and thus improved electronic contact between electrode materials [32]. Fig.8 shows the cycle performance of AC/$LiFePO_4$ and ACNF/$LiFePO_4$ electrodes at 0.20 C. The AC/$LiFePO_4$ electrode delivered higher discharge capacities (45 mA hg^{-1}) than that of the ACNF/$LiFePO_4$ electrode (5 mA hg^{-1}) after 50^{th} cycles at 0.20 C. The high discharge capacity of the AC/$LiFePO_4$ electrode could have been caused by the synergistic effect between materials. The distribution of $LiFePO_4$ nanoparticles wrapped with a carbon sheet matrix may have been better than that of non-woven carbon nanofibers.

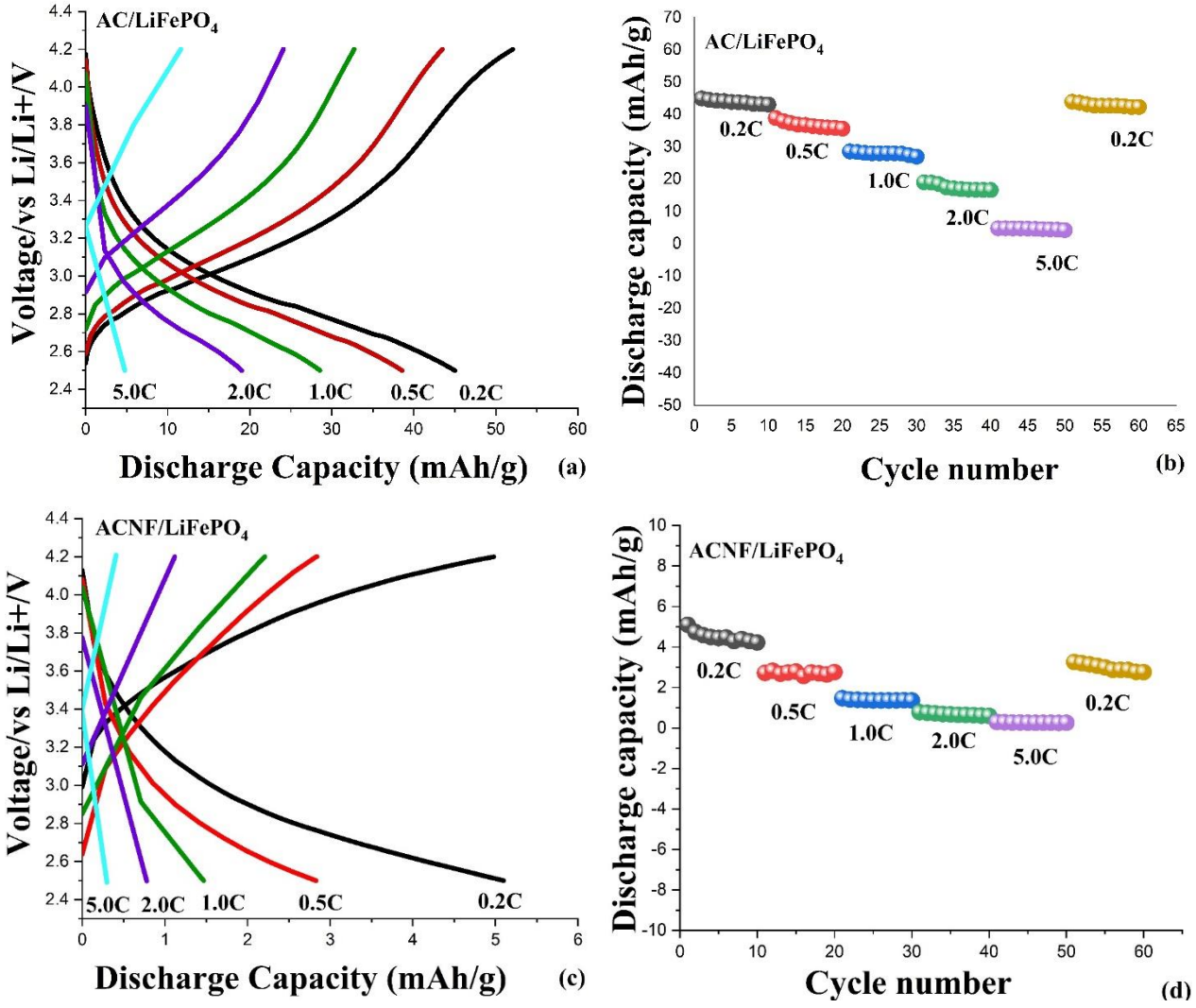

Fig. 7 First charge-discharge profiles of (a) AC/$LiFePO_4$ and (c) ACNF/$LiFePO_4$ electrodes. The rate capability of (b) AC/$LiFePO_4$ and (d) ACNF/$LiFePO_4$ electrodes.

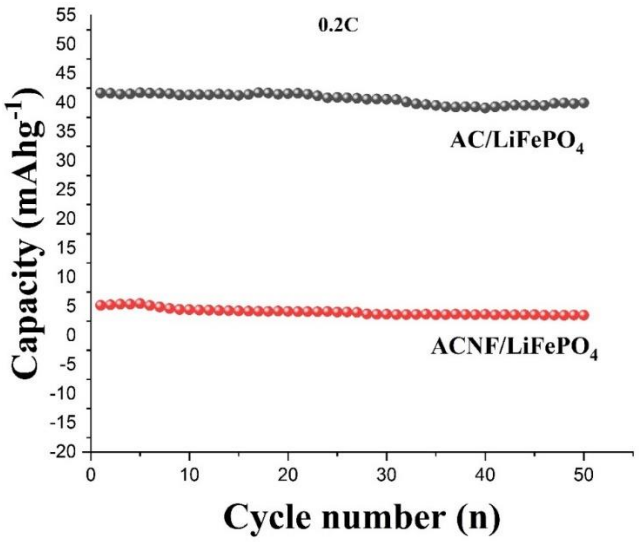

Fig. 8 Cycle performance of $AC/LiFePO_4$ and $ACNF/LiFePO_4$ electrodes at 0.20 C.

Conclusion

Activated carbon nanofiber/lithium iron phosphate composite nanostructures **(**$ACNF/LiFePO_4$**)** and activated carbon /lithium iron phosphate composite nanostructures **(**$AC/LiFePO_4$**)** were synthesized using electrospinning and sol-gel methods, respectively, followed by the heat treatment process. The prepared sample exhibited a uniform nanosphere shape of $LiFePO_4$ with an average particle size below 300 nm embedded in the porous carbon matrix. The $AC/LiFePO_4$ electrode presented better electrochemical properties than those of the $ACNF/LiFePO_4$ electrode. A maximum specific capacitance of 82 F g^{-1} was observed at 2 m Vs^{-1}**.** An initial discharge capacity of 45 mA hg^{-1} was observed at **0.**20 C. Moreover, the $AC/LiFePO_4$ electrode showed better cycle performance than that of the $ACNF/LiFePO_4$ electrode at all C-rates. Good electrochemical performance of $AC/LiFePO_4$ may be assigned to (i) the formation of well-distributed activated carbon matrix (AC) around $LiFePO_4$ making great electronic interconnections (ii) the nanoscale of $LiFePO_4$ particle size reducing the diffusion distance of electron/ions and (iii) the high surface area supporting a large number of sites for electrolyte ions penetration. The interesting electrochemical properties of $AC/LiFePO_4$ composite nanostructure make it a potential candidate for use as electrode materials in energy storage devices.

Acknowledgements

This research project is supported by Thailand Science Research and Innovation **(**TSRI**).** Contract No. FRB650059/NMA/13**.** The authors are thankful to the department of Applied Physics Rajamagala University of Technology Isan **(**RMUTI**)** and Synchrotron Light Research Institute **(**Public Organization**)**: SLRI for providing all the facilities.

References

[1] N. Bugday, M.N. Ates, O. Duygulu, W. Deng, X. Ji, S. Altin, S. Yasar, ZIF-12-derived N-doped Fe/Co/S/@C nanoparticles as high-performance composite anode electrode materails for lithium-ion batteriers, J. Alloys Compd. 928 (2022) 167037.

[2] Ya. V. Shatilo, E.V. Makhonina, V.S. Pervov, V.S. Dubasova, A.F. Nikolenko, Zh. V. Dobrokhotova, and I.A. Kedrinskii, LiCoO2- and $LiMn_2O_4$-Based Composite Cathode Materials, Inorg. Mater. 42(7) (2006) 782 − 787.

[3] P. Kurzhals, F. Riewald, M. Bianchini, H. Sommer, H.A. Gasteiger, and J. Janek, The $LiNiO_2$ Cathode Active Material: A Comprehensive Study of Calcination Conditions and their Correlation with Physicochemical Properties. Part I. Structural Chemistry, J. Electrochem Soc. 168 (2021) 110518.

[4] [A.K. Padhi, K.S. Nanjundaswamy, J.B. Goodenough, Phospho-olivines as positiveelectrode materials for rechargeable lithium batteries, J. Electrochem. Soc. 144 (1997) 1188 − 1194.

[5] E.C. Evarts, Lithium batteries: To the limits of lithium. Nature 526 (2015) S93 − S95.

[6] R. Susantyoko, T.S. Alkindi, A.B. Kanagaraj, B. An, H. Alshibli, D. Choi, S. Aldahmani, H. Fadaq, S. Almheiri, Performance optimization of freestanding MWCNF-$LiFePO_4$ sheets as cathodes for improved specific capacity of lithium-ion batteries. RSC Adv 8 (2018) 16566 − 16573.

[7] Y. Liu, J. Liu, J. Wang, M.N. Banis, B. Xiao, A. Lushington, W. Xiao, R. Li, T.K. Sham, G. Liang, X. Sun, Formation of size-dependent and conductive phase on lithium iron phosphate during carbon coatin, Nat. Commun. 9 (2018) 1 − 8.

[8] H.C. Shin, K.Y. Chung, W.S. Min, D.J. Byun, H. Jang, B.W. Cho, Asymmetry between charge and discharge during high rate cycling in $LiFePO_4$– In Situ X-ray diffraction study, Electrochem. Commun. 10 (2008) 536 − 540.

[9] A. Eftekhari, $LiFePO_4$/C nanocomposites for lithium-ion batteries J. Power Sources. 343 (2017) 395 − 411.

[10] Kang B, Ceder G. Battery materials for ultrafast charging and discharging, Nature. 458 (2009) 190 − 193.

[11] C.S. Sun, Y. Zhang, X.J. Zhang, Z. Zhou, Structural and electrochemical properties of Cl-doped $LiFePO_4$/C, J. Power Sources 195 (2010) 3680 − 3863.

[12] N. Ye, T. Yan, Z. Jiang, W. Wu, T. Fang, A review: conventional and supercritical hydro solvothermal synthesis of ultrafine particles as cathode in lithium battery, Ceram. Int. 44 (2018) 4521 − 4537.

[13] Y. Tang, F. Huang, H. Bi, Z. Liu, D. Wan, Highly conductive three-dimensional graphene for enhancing the rate performance of $LiFePO_4$ cathode. J. Power Sources. 203 (2012) 130 − 134.

[14] M. Khalid, Ana M.B. Honorato, A.A. Pasa, H. Varela, A sugar derived carbon-red phosphorus composite for oxygen evolution reaction and supercapacitor activities, Materials Science for Energy Technologies, 3 (2020) 508 − 514.

[15] J. Lee, W. Kim, W. Kim, Stretchable carbon nanotube/ion–gel supercapacitors with high durability realized through interfacial microroughness, ACS Appl. Mater. Interfaces 6 (16) (2014) 13578-13586.

[16] S. Nilmoung, W. Limphirat, S. Maensiri, Electrochemical properties of ACNF/Li_2FeSiO_4 composite nanostructures for supercapacitors. J. Alloys Compd. 907 (2022) 164466.

[17] H. Yang, S. Kannappan, A.S. Pandian, J.H. Jang, Y.S. Lee, W. Lu, Graphene supercapacitor with both high power and energy density, Nanotechnology, 28(44) (2017) 445401.

[18] Y.Huang, H. Lai, Effects of discharge rate on electrochemical and thermal characteristics of $LiFePO_4$/graphite battery, Appl. Therm. Eng. 157 (2019) 113744.

[19] V.A. Streltsov, E.L. Elokoneva, V.G. Tsirelson, N.K. Hansen, Multipole analysis of the electron density in triphylite $LiFePO_4$, using X-ray diffraction data, Acta Crystallogr, B 49 (1993) 147-153.

[20] S. Shen, Y. Zhang, G. Wei, W. Zhang, X. Yan, G. Xia, A. Wu, C. Ke, and J. Zhang, Li_2FeSiO_4/C hollow nanospheres as cathode materials for lithium-ion Batteries, Nano Res. 12(2) (2019) 357 − 363.

[21] W. Wang, P. Liu, M. Zhang, J. Hu, F. Xing, The pore structure of phosphoaluminate cement, Open J. Compos. Mater. 2 (2012) 104 – 112.

[22] L. Hea, W. Zha, D. Chena, Fabrication and electrochemical properties of 3D nano-network LiFePO4@multiwalled carbon nanotube composite using risedronic acid as the phosphorus source, Prog. Nat. Sci. 29 (2019) 156 − 162.

[23] P. Rosaiah, O.M. Hussain, Microscopic and spectroscopic properties of hydrothermally synthesized nano-crystalline $LiFePO_4$ cathode material, J. Alloys Compd. 614 (2014) 13 − 19.

[24] B. Yao, Z. Ding, J. Zhang, X. Feng, L. Yin, Encapsulation of $LiFePO_4$ by in-situ graphitized carbon cage towards enhanced low temperature performance as cathode materials for lithium ion batteries, J. Solid-State Chem. 216 (2014) 9 − 12.

[25] S. Dhaybi, B. Marsan, A. Hammami, A novel low-cost and simple colloidal route for preparing high-performance carbon-coated $LiFePO_4$ for lithium batteries, J. Energy storage 18 (2018) 259 − 265.

[26] C.K. Lee, A.S.T. Chiang, C.S. Tsay, The characterization of porous solids from gas adsorption measurements, Key Eng. Mater. 115 (1995) 21 − 44.

[27] M. Salanne, B. Rotenberg, K. Naoi, K. Kaneko, P.-L. Taberna, C.P. Grey, B. Dunn, P. Simon, Efficient storage mechanisms for building better supercapacitors, Nat. Energy 1 (2016) 1 − 10.

[28] J. Li, D.B. Le, P.P. Ferguson, J.R. Dahn, Lithium polyacrylate as a binder for tin-cobalt-carbon negative electrodes in lithium-ion batteries, Electrochim. Acta. 55(8) (2010) 2991-2995.

[29] M.K. Sahoo, G.R. Rao, Fabrication of $NiCo_2S_4$ nanoball embedded nitrogen doped mesoporous carbon on nickel foam as an advanced charge storage material, Electrochim. Acta 268 (2018) 139 − 149.

[30] S. Sarkar, and S. Mitra, Carbon coated submicron sized-$LiFePO_4$: Improved high rate performance lithium battery cathode, Energy Procedia 54 (2014) 718 − 724.

[31] H. Zhang, G.R. Li, L.P. An, T.Y. Yan, X.P. Gao, H.Y. Zhu. Electrochemical lithium storage of titanate and titania nanotubes and nanorods. J. Phys. Chem. C. 111 (2007) 6143 − 6148.

[32] V. Gangaraju, M. Shastri, K. Shetty, N.R. Marilingaiah, K.S. Anantharaju, P.D. Shivaramu, D. Rangappa, In-situ preparation of silk-cocoon derived carbon and $LiFePO_4$ nanocomposite as cathode material for Li-ion battery, Ceram. Int. 48 (2022) 35657 − 35665.